Journal of Scientific & Industrial Research
Vol. 84, May 2025, pp. 584-600
DOI: 10.56042/jsir.v84i5.15048

Performance Analysis of Hybrid Mixed Line Rate Nyquist Super Channel Transmission of Unicast and Multicast Overlay System

Deepak Sahu & Chakresh Kumar*

University School of Information, Communication & Technology, Guru Gobind Singh Indraprastha University, New Delhi, 110 078, India

Received 13 November 2024; revised 13 February 2025; accepted 13 March 2025

Internet-based services such as email, file transfer protocols, real-time applications, and on-demand content delivery systems like Netflix exemplify unicast data transmission. Applications such as the dissemination of online class, software updates, IoT-based system control messages and connectivity for various applications, and collaborative platforms like online gaming and virtual reality environments necessitate a multicast data transmission system. This research investigates the performance of a mixed line rate combined with Nyquist transmission. This system features subcarrier-based super-channel subsystems that incorporate polarization mixed 8-Quadrature amplitude modulation (PM-8QAM) 166 Gb/s data rate and Nyquist dual polarized 16-Quadrature amplitude modulation system (Nyquist DP-16QAM). A 112 Gb/s data rate WDM super channel, combined with a 56 Gb/s POLSK-based system, creates a Unicast super channel. Eight multiple sub-carrier-based unicast super-channels are formed and blended with the Multicast system that uses differential quadrature phase shift keying (DQPSK) for 56 Gb/s multicast transmission. The system transmits 5.856 Tb/s of total data rate via 8 × 725 Gb/s unicast and 56 Gb/s multicast signals. The simulation results were used to determine the BER, input power, and Q-factor for the multicast overlay system. The results obtained showed high Q values, low BER, and great spectral efficiency across a distance of 600 Km.

Keywords: Coherent detection, Dual polarization, Mixed line rate modulation, Polarization mixing, Strokes parameters

Introduction

Various modulation schemes like NRZ, duobinary, DQPSK, and SDPSK have been proposed for 100Gbits applications. Propagation of blended 260-Gb/s PDM-16QAM and 130-Gb/s PDM-QPSK signals over 950-km and 4200-km dispersion-managed (DM) SSMF spans is examined. The effects of pulse shaping, temporal interleaving polarisations, and maximum likelihood (ML) detection on system performance is investigated. The study concluded that these approaches boost nonlinear transmission performance, boosting the reach of PDM-16QAM by 40% and PDM-QPSK by 10%. Effective transmission is demonstrated with 23% overhead hard-decision FEC, illustrating the viability of high-speed mixed-modulation systems in DM fiber lines.[1] 450-Gb/s dual-carrier PDM-16QAM transmission in a 75-GHz WDM grid with a spectral efficiency of 6 b/s/Hz is demonstrated. Optic pre-filtering and RZ wave structuring augment performance without Nyquist filtering or OFDM, resulting in a 678 km broadcast range.[2] A new code formulation algorithm for 3D Optical Code Division Multiple Access (OCDMA) that leverages space-wavelength-time codes is offered. The suggestion that multiple pulses per plane (MPP) codes optimise cross-correlation, diminishing multiple access interference (MAI) and enhancing bit error rate (BER). The study explores the influence of multiple temporal lengths and cardinality on performance. The results illustrate that the proposed 3D codes deliver a BER below 10^{-13}, outperforming earlier approaches. This technique optimises OCDMA efficiency in asynchronous optical fiber communication networks.[3] The functionality of Optical CDMA (OCDMA) systems using 2D optical codes is examined by comparing prime hop and hybrid codes to correlation conventional receiver (CCR) and serial interference cancellation (SIC) receivers. It illustrates that SIC receivers notably lessen multiple access interference (MAI) while boosting system performance. A five-stage SIC receiver can support over 900 concurrent users with a BER of 10^{-10}, in contrast to 550 with a CCR. The study emphasises on crucial aspects such as prime number selection, threshold optimisation, and

*Author for Correspondence
E-mail: chakreshk@ipu.ac.in

multiuser detection that could enhance OCDMA performance.[4] A survey of advances in all-optical spectral amplitude coding algorithms for Optical Code Division Multiple Access (OCDMA) systems is presented. It compares the efficiency of various spectral amplitude codes (SACs), such as Walsh-Hadamard, Multi diagonal, Modified Double Weight, and Enhanced Double Weight codes, in terms of bit error rate (BER), signal-to-noise ratio (SNR), and system security. The article determines issues such as multiple access interference (MAI) and security risks, while proposing changes to improve performance.[5] The research effort explores a hybrid WDM-OTDM optical multicast overlay network that uses 120 Gbps polarisation and subcarrier multiplexed unicast data, as well as 50 Gbps DPSK multicast data. The study investigates how extinction ratio, input power, and transmission distance influence system efficiency in terms of BER, optical power, and Q-factor. The findings reveal that polarisation and subcarrier multiplexed modulation schemes enhance spectral efficiency while diminishing chromatic and polarisation mode dispersion. The implied technology boosts bandwidth usage and permits reliable data transfer across 150 km.(6) The research describes and analyses an asynchronous digital optical regenerator (ADORE) that employs a single electro-absorption modulator (EAM) loop and a neighbour-combine technique. This device successfully re-synchronizes input signals with arbitrary phases to the local clock, thereby decreasing amplitude inconsistencies and polarisation mode dispersion. The study clarifies how to convert 4 × 40 Gbit/s WDM signals to 160 Gbit/s OTDM format. The proposed ADORE optimises signal regeneration, timing, and pulse rearrangement for rapid connectivity optical links.[7] The research analyses a 4.0 Tbps packed wavelength division multiplexed (DWDM) system that implements a hybrid encoding tackle connecting NRZ, DQPSK, and PolSK. A 30 × 110 Gbps channel structure with 30 GHz separation is shown to effectively transmit over 50 kilometres using limited resource occupancy (0.75 THz). The suggested strategy is appropriate for fast optical networks, as evidenced by acceptable BER ($<10^{-10}$) and received power (> -45 dBm).[8] The study shows the transmission of a 300-Gb/s orthogonal PDM-RZ-QPSK DWDM signal across 1040 km of SMF fiber. The technology achieves a BER of less than 2.3×10^{-4} without Raman amplification or optical dispersion compensation through precise optical filtering and polarisation combining. The necessary OSNR for error-free transmission is 24 dB, which indicates the viability of high-speed, chromatically effective DWDM transport.[9] The research presents a 100 Gbit/s three-dimensional orthogonal modulation scheme which incorporates Dark RZ (DRZ), DQPSK, and PoISK to boost spectral effectiveness and transport resilience. When juxtaposed with DQPSK, numerical models show that PMD and chromatic dispersion are more bearable. The method offers a limited spectrum and good susceptibility to phase noise, making it an appealing choice for fast-speed optical links.[10] The study offers a 0.50 Tb/s multimodal Nyquist-WDM super channel featuring polarization-multiplexed BPSK, QPSK, 8-QAM, and 16-QAM subcarriers that operated at 30 Gbaud. It achieves great spectral efficiency (5 b/s/Hz) and a transmission range of 6000 km for PM-QPSK and 2300 km for PM-16QAM over pure silicon core fiber (PSCF). Hybrid optical enhancement with Raman and EDFA reduces OSNR specifications, rendering it cost-effective and beneficial for long-haul high-capacity network connections.[11] The research examines the efficiency of grey-coded IQM-based photonic modulation schemes (QPSK, 16-QAM, 32-QAM, and 64-QAM) in rapid long-haul optical communications. Grey-coded methods outweigh differential-coded systems with regard to of OSNR demand, receiver sensitivity, and transmission reach, with QPSK attaining up to 6500 km and 64-QAM achieving 400 km. Sophisticated DSP algorithms mitigate for fiber impairments, strengthening system performance for rapid transfer.[12] The study presents a thorough examination of coherent optical fiber communications, including the fundamentals of uniformity detection, quantum noise features, and DSP strategies. It tackles the benefits of coherent recipients, such as rectifying for linear deficiencies and permitting extremely efficient spectral modulation methods like QAM. The paper highlights improvements to DSP algorithms for carrier phase estimation, polarisation tracking, and dispersion compensation, which are critical for next-generation high-speed optical networks.[13] The research shows an adaptable terabit/s Nyquist-WDM super-channel utilising a gain-switched comb source that delivers 2.2 Tbit/s transmission over 120 km and 2.6 Tbit/s over 250 km. The technique uses polarization-multiplexed QPSK and 16QAM modulation with configurable comb line separation to achieve great

spectral effectiveness (up to 8 b/s/Hz). The recommended approach delivers security, flexibility, and affordability for fast optical network connections.[14] The research presents a capacity-constrained ultimate temporally detached lightpath (CMSDL) method for following a catastrophe lightpath recovery in flexible optical links. The program effectively redirects obstructed links by using minimally loaded and aesthetically disjunct pathways, reducing latency and boosting link success. Simulation findings indicate minimised blockage likelihood and better utilisation of resources than normal protection approaches, which enhances network adaptability in situations of catastrophe.[15] The investigation focusses at 100 Gb/s consistent NG-PON2 southbound communication utilising polarization-multiplexed modulation techniques (PM-BPSK, PM-QPSK, and PM-16QAM). It assesses functionality across 15–75 km fiber utilising various partition proportions, evaluating the recipient sensitivity, BER, OSNR, and resource budget. Digital signal processing (DSP) remedies for fiber imperfections, enabling outstanding data speeds alongside effective delivery for future optical network construction.[16] The research exhibits spectrally operational WDM transfer with Nyquist pulse-shaped 16-QAM subcarrier encoding and explicit sensing. A 6×20 GHz-spaced WDM scheme has a net data rate of 24 Gb/s per channel and a spectral performance of 1.2 b/s/Hz over 290 km of traditional single-mode fiber. The study illustrates economical, high-capacity optical interaction for urban and local networks.[17] The research investigates the effect of ageing optical boosters on flex-grid optical links, in which reduced channel spacing enhances the total number of optical channels. It suggests a link approach to design which employs power adjustment for optimal wavelength effectiveness while conserving legacy equipment. The study demonstrates that controlling launch power permits smooth network relocation despite the need for expensive amplifier upgrades.[18] To improve the efficiency of the spectral spectrum, the research offers a Nyquist WDM super channel that uses offset-16QAM and receiver-side digital spectrum structuring (RS-DSS). The technology achieves 7.5 b/s/Hz spectral efficiency and 1.6 dB OSNR improvement at BER = 10^{-4} compared to traditional 16QAM-based RS-DSS. It demonstrates reliable transmission over 1000 km SSMF using EDFA-only enhancement, which enhances phase fluctuation sensitivity for practical installation.[19] The research looks at the effectiveness of Nyquist-WDM terabit super channels employing PM-BPSK, PM-QPSK, PM-8QAM, and PM-16QAM subcarriers. It compares wavelength effectiveness and broadcast reach, revealing that PM-BPSK penetrates 6590 km at 3.9 Tb/s, but PM-16QAM supports 30 Tb/s but only reaches 250 km. The study focusses on the trade-offs among throughput and accessibility in contemporary optical links.[20] The research reports a record 40 Tb/s C-band transfer rate leveraging PM-64QAM throughout 800 km of field-deployed SSMF utilising composite EDFA-Raman augmentation. It also achieves 25.0 Tb/s with PM-16QAM and 35 Tb/s with PM-32QAM, with the spectral efficiency enhanced up to 7.8 b/s/Hz. The findings support the potential of high-capacity, flexi-rate terabit super channels in long-haul optical links.[21] The research presents a bandwidth-efficient WDM-PON system that allows concurrent transmission of 70 Gb/s single-cast and 20 Gb/s multiplex amenities via asymmetric modulation (NRZ/PolSK and DPSK). It exhibits reliable transmission for 30 kilometres with satisfactory parameters and BER. The technique enhances the utilisation of spectrum while minimising power consumption, making it appropriate for rapid optical connections.[22] The study describes a 1.51 Tb/s Nyquist-WDM super channel that uses five 212 Gb/s PM-16QAM subcarriers with a functional effectiveness of 7.12 b/s/Hz. It uses Nyquist pre-filtering to reduce inter-channel interference, resulting in a BER of 3×10^{-4} at 24 dB OSNR over a 150 km fiber. The suggested technology improves spectrum efficiency and is appropriate for future, high-capacity optical networks.[23] The research investigates the effects of bit rate, spectrum, and energy on the quality factor and BER in Free Space Optics (FSO) systems. The simulation results suggest that a 5.0 Gbit/s bit rate, 1530 nm wavelength, and 10 dBm power produce an ideal quality factor of 85. The study highlights the significance of parameter tuning for boosting FSO system efficiency.[24] The work presents an empirical investigation of BER estimation for PAM-N and M-QAM modulation employing single-sideband (SSB) signals. It determines quantitative BER expressions employing OSNR and CSPR to simulate different detection methods such as IM/DD, coherent detection, and SSB-DD. Simulations using 212 Gb/s SSB-PAM4/16QAM corroborate the theoretical models, facilitating system optimising for rapid connectivity communication via optics.[25]

In this paper, a new design of a mixed line rate, Nyquist flexible system with a multicast overlay system is proposed that uses differential quadrature phase shift keying (DQPSK) for 56 Gb/s of multicast data and mixed line rate comprising of Nyquist dual polarisation quadrature amplitude and polarized multiplexed (DP-16QAM & PM 8QAM) modulation is used for 725 Gb/s of unicast data transmission. The design of 5.856 Tb/s data transmission employing 8 × 725 Gb/s unicast and 56 Gb/s multicast signals, with a minimum BW 0.015 THz band gap utilization in each subchannel of Nyquist DP-16QAM & PM-8QAM modulation, is proposed in this work.

Mathematical Analysis

Nyquist Pulse Shaping

Consider a sample period T_{Nqs} as given in Eq. (1) and an integer progressive value n the time domain magnitude representation in a most basic way can be represented as given in Eq. (1).

$$h(nT_{Nqs}) = \begin{cases} 1 & n = 0 \\ 0 & n \neq 0 \end{cases} \quad \ldots (1)$$

Considering the diagrammatic representation of a sample spaces time domain of Nyquist pulse in Fig. 1(a), it is observed that the maximum value occurs at time t = 0 whereas at all other points, it shows a diminishing null value just like damped harmonics which corresponds to $t = n.T_{Nqs}$. Frequency domain Nyquist characteristics is shown in Eq. (2) where the Fourier transform representation of h(t) is given, k is integer.

$$\frac{1}{T_{Nqs}} \sum_{k=-\infty}^{\infty} H\left(f - \frac{k}{T_{Nqs}} \right) = 1 \quad \ldots (2)$$

The mathematical representation of the frequency domain when interpreted in the form of pictorial representation is shown in Fig. 1(b).

A general basic representation of Nyquist pulse can be given as shown in Eq. (3) whose diagrammatic representation is represented in Fig. 2(a). Eq. (3) represents the impulse response of a raised cosine Nyquist filter.

$$h(t)_{Nyquist} = \frac{\sin\left(\frac{2\pi t}{T_{nqs}}\right)}{\frac{2\pi t}{T_{nqs}}} \cdot \frac{\cos\left(\frac{R_{rate}\pi t}{T_{nqs}}\right)}{1 - \left(\frac{2R_{rate}\pi t}{T_{nqs}}\right)^2} \quad \ldots (3)$$

As mentioned in Eq. (3) $h(t)_{Nyquist}$ represents the amplitude of the Nyquist pulse, R_{rate} is a roll-off factor of the Nyquist pulse which lies in the range $0 \leq R_{rate} \leq 1$, T_{nqs} sample duration where the first zero crossing occurs. In pictorial form, Eq. (3) is

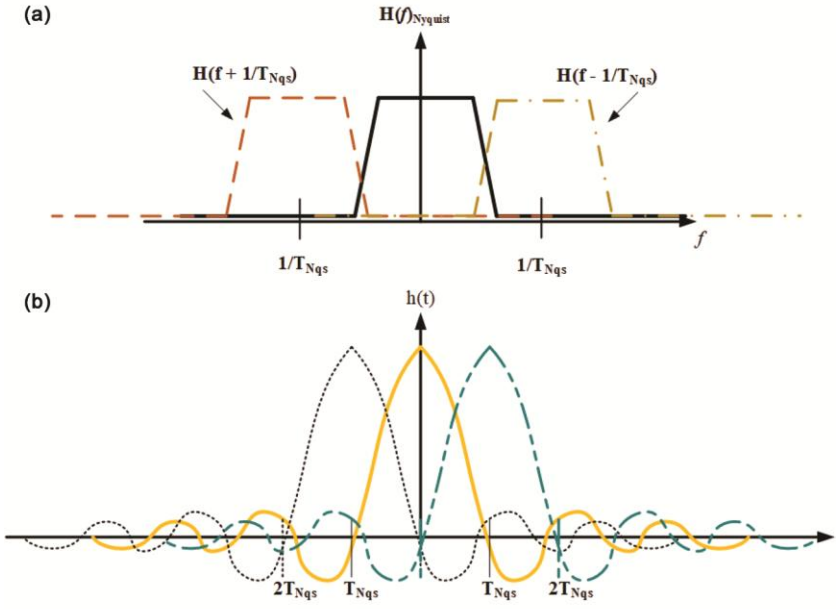

Fig. 1— (a) Raised cosine response (at centre bold at t = 0) meets ISI criteria, all other dashed lines show various sampling instants in frequency domain, and (b) time domain representation Nyquist pulse in sin*c* form all adds up to a constant

represented as shown in Fig. 2(a), which is characterized by the value of the roll-off rate factor R_{rate}. Considering roll-off rate effect first it can be related with bandwidth, when R_{rate} is equal to zero, a minimum bandwidth condition is achieved which is equal to the Nyquist rate. In this half the symbol rate is there i.e., $\frac{1}{2T_{Nqs}}$, where T_{Nqs} is the sampling period. Further in the frequency domain generation of desired rectangular pulses are represented in Eq. (4). The diagrammatic representation of superimposed pulses is shown in Fig. 2(b)

$$H(f)_{Nyquist} = \begin{cases} T_{nqs} & |f| \le \frac{1-R_{rate}}{2T_{nqs}} \\ \frac{T_{nqs}}{2}\left[1+\cos\left(\frac{\pi T_{nqs}}{R_{rate}}\left[|f| \le \frac{1-R_{rate}}{2T_{nqs}}\right]\right)\right] & \frac{1-R_{rate}}{2T_{nqs}} \le |f| \le \frac{1+R_{rate}}{2T_{nqs}} \\ 0 & otherwise \end{cases} \quad \ldots (4)$$

which gives a series of rectangular pulses where message signals are transmitted. For values of roll-off rate between zero and one the bandwidth of the filter increases, this increase varies from the Nyquist rate to double that of the Nyquist rate. The total resultant bandwidth is given by $\frac{1+R_{rate}}{2T_{Nqs}}$. The frequency domain representation for a variation of the roll-off rate is shown in Fig. 2(b). Nyquist and raised cosine filter in mathematical form can be related as shown in Eq. (5).

$$H_R(f) = H_T(f) = \left|\sqrt{H(f)}\right| \text{ where terms are RCF and Nyquist filter} \quad \ldots (5)$$

Differential Quadrature Shift Keying

The differential coding techniques are very similar to differential phase shift keying, the difference what it incorporates is that along with the two bits that are present in orthogonal discrete value spaces having a phase variation of $0 \to \pi$ in addition to this there are two sets of bits on imaginary axis having variation of $-\pi/2 \to \pi/2$ as shown in Fig. 3(a).

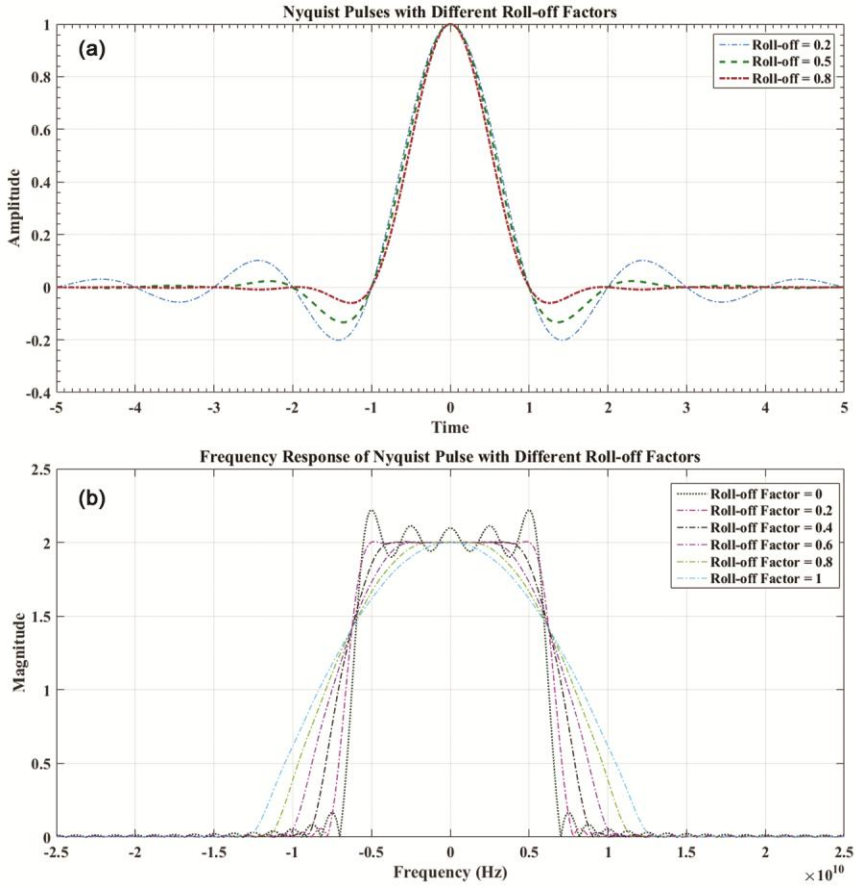

Fig. 2 — (a) magnitude h(t) of Nyquist Sin(c) pulse for different roll-off factors in the time domain, and (b) magnitude H(f) of Nyquist Sin*c* pulse for different roll-off factor in the frequency domain

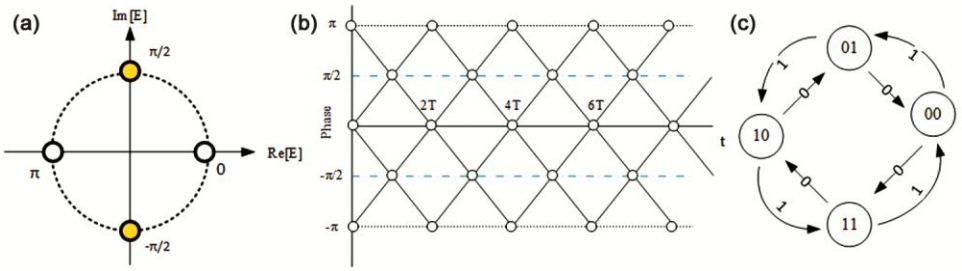

Fig. 3 — (a) DQPSK constellation diagram, (b) MSK Phases lattice distribution, and (c) state diagram

Minimum Shift Keying

In MSK two frequencies are placed in a systematic manner such that they are orthogonal and have the least required spacing which in mathematical form can be given as mentioned in Eq. (6).

$$x(t)_{sym1} = \sqrt{\frac{U_{bit}}{T_{bit}}}\cos\left(2\pi f_{sym1}t + q(0)\right) \qquad \textit{for symbol 1}$$

… (6)

The mentioned Eq. (6) represents the transmission of symbol '1' bit and the frequency used in this is represented by f_{sym1} whose value is given as shown by Eq. (7) in this '1' bit is responding to higher frequency changes

$$f_{sym1} = f_{carrier} + \frac{1}{4.T_{bit}} \qquad \text{… (7)}$$

$$x(t)_{sym0} = \sqrt{\frac{U_{bit}}{T_{bit}}}\cos\left(2\pi f_{sym2}t + q(0)\right) \qquad \textit{for symbol 0}$$

… (8)

The mentioned Eq. (8) represents the transmission of symbol '1' bit and the frequency used in this is represented by f_{sym1} whose value is given as shown by Eq. (9) in this '1' bit is responding to lower frequency changes

$$f_{sym2} = f_{carrier} - \frac{1}{4.T_{bit}} \qquad \text{… (9)}$$

depending on binary data the phase of the signal changes for bit '1', it increases in phase by value $\pi/2$ and respectively there is a decrease in phase of value $\pi/2$ for bit '0'. The changes evolved in carrier frequency from having changed from '0' to '1' and vice-versa is equal to half of the incoming bit rate. Minimum frequency spacing that allows both signals to be represented orthogonally. The phase variation is represented by straight lines in the phase matrix slope of lines is used as frequency changes. Now the changes that occur in carrier frequency from data changing from '0' to '1' or vice-versa are observed to be half of the bit rate of incoming data. An MSK signal consists of both 'I' and 'Q' components which can be given in numerical formulations represented in Eq. (10).

$$x(t) = \sqrt{\frac{U_{bit}}{T_{bit}}}\cos\left(2\pi f_{carrier}t\right)\cos\left(q(t)\right) - \sqrt{\frac{U_{bit}}{T_{bit}}}\sin\left(2\pi f_{carrier}t\right)\sin\left(q(t)\right)$$

… (10)

The in-phase component has half-sine pulses represented mathematically as mentioned in Eq. (11).

$$x_I(t) = \pm\sqrt{\frac{2.U_{bit}}{T_{bit}}}\cos\left(\frac{\pi t}{2T_{bit}}\right) \qquad -T_{bit} \le t \le T_{bit}$$

… (11)

The quadrature component has the form as described by Eq. (12).

$$x_Q(t) = \pm\sqrt{\frac{2.U_{bit}}{T_{bit}}}\sin\left(\frac{\pi t}{2T_{bit}}\right) \qquad 0 \le t \le 2T_{bit} \qquad \text{… (12)}$$

Considering the duration of an even bit interval, the I component for '0' will have a +ve cosine waveform whereas a negative cosine for a phase of π, and so on for odd bit duration Q component has a positive sin waveform for value $\pi/2$ and its negative pair has a phase of $-\pi/2$. Out of all 4 combinations 0, $\pi/2$, $-\pi/2$, π. The resultant transmitted pulse is the combination of I and Q components and the phase is continuous in time. All this is represented in Fig. 3(b) and Fig. 3(c). Now one of the major characteristics of minimum shift keying is that data is minimum being held for two bits time duration which results in a symbol rate of two bits. A delay on bit is there between the I and Q components therefore only one of them can change at a time which means that if one is at zero crossing other will be present there at maximum peak.

Polsk (Polarization Shift Keying) Modulation

Light being an electromagnetic wave can be split into two orthogonal components which are primarily

in the x and y direction considering the wave is travelling in the z direction.

$$\psi_x = m_x(t).e^{\{i(\omega t+\varphi_x(t)\}}.\hat{x} \quad \ldots (13)$$

$$\psi_y = m_y(t).e^{\{i(\omega t+\varphi_y(t)\}}.\hat{y} \quad \ldots (14)$$

where, ω is the angular frequency, m is the magnitude of the component magnitude and φ being the phase of orthogonal components. The x and y direction components of an electromagnetic wave that is travelling in the z-direction are presented by the Eqs (13–14). A conventional representation for the state of polarization is indicated using Strokes parameters defined in a basic representation as given in Eq. (15) which represents strokes parameters.

$$\vec{S}_{strokes} = \begin{pmatrix} S_{st0} \\ S_{st1} \\ S_{st2} \\ S_{st3} \end{pmatrix} = \begin{pmatrix} I_{st} \\ Q_{st} \\ U_{st} \\ V_{st} \end{pmatrix} \quad \ldots (15)$$

some common states of polarization are mentioned as in Eq. (16).

$$\begin{pmatrix} S_{st0} \\ S_{st1} \\ S_{st2} \\ S_{st3} \end{pmatrix} = \begin{pmatrix} 1 \\ 1 \\ 0 \\ 0 \end{pmatrix}_{Linearly\ Polarized} = \begin{pmatrix} 1 \\ -1 \\ 0 \\ 0 \end{pmatrix}_{Linearly\ Polarized(vertical)}$$

$$= \begin{pmatrix} 1 \\ 0 \\ 1 \\ 0 \end{pmatrix}_{Linearly\ Polarized(+45^o)} = \begin{pmatrix} 1 \\ 0 \\ -1 \\ 0 \end{pmatrix}_{Linearly\ Polarized(+45^o)} \quad \ldots (16)$$

$$S_{st0} = I_{st} = \psi_x{}^2 + \psi_y{}^2 \quad \ldots (17)$$

In Eq. (16) S_{st0} is the optical intensity. S_{st1} shown in Eq. (18) represents the intensity difference between horizontal and vertically polarized components. When S_{st1} it has a positive value then there is an occurrence of horizontal polarization which constitutes a linear polarized wave in the x direction. When it is negative there is an occurrence of vertical Polarization which constitutes a linear polarized wave in the y direction.

$$S_{st1} = Q_{st} = \psi_x{}^2 - \psi_y{}^2 \quad \ldots (18)$$

S_{st2} given in Eq. (19) represents the preference for -45° or +45° state of polarization. A positive value indicates an inclination for +45° whereas a negative value indicates an inclination for −45°.

$$S_{st2} = U_{st} = 2.\psi_x.\psi_y \cos(\phi) \quad \ldots (19)$$

S_{st3} represents the right-hand circular and left-hand circular polarization. A positive value indicates inclination for right circular whereas a negative value indicates left circular polarization.

$$S_{st3} = V_{st} = 2.\psi_x.\psi_y \sin(\phi) \text{ where } \phi = \varphi_x(t) - \varphi_y(t) \quad \ldots (20)$$

Every possible combination of state of polarization can be represented using the Poincare Sphere where strokes component S_{sti} having i value to be 1, 2, 3 are normalized by the intensity component S_{st0}. As shown in Fig. 4(a) Poincare sphere at the equator represents various forms of linear polarization. Right-hand and left-hand circular polarization are represented at the top of spheres where RHC is at the northmost pole and LHC is at south southmost pole. Points at the opposite end of the line passing through the center represent orthogonal polarization as indicated in Fig. 4(b). There is also another way to represent stroke vectors with the state of polarization which is represented as mentioned in Eq. (21).

$$S_{st1} = \cos 2\phi.\cos 2\theta \quad \ldots (21)$$

where, 2ϕ represents the azimuthal angle or it can be represented as orientation having variation from $+\pi/2 \rightarrow -\pi/2$ whereas 2θ represents the elliptical angular vales having angular variation from $+\pi/4 \rightarrow -\pi/4$.

$$S_{st2} = \sin 2\phi.\cos 2\theta \quad \ldots (22)$$

The points of the Poincare sphere are represented using two angular forms of azimuthal and ellipticity as shown in Fig. 4(c) and in tabular form various polarization states and Strokes parameters are related along with the Azimuthal angle and Ellipticity variation as shown in Fig. 4(d).

$$S_{st3} = \sin 2\theta \quad \ldots (23)$$

System Set up

In the first part as shown in Fig. 5(a), five mixed line rate subcarriers are shown. At the odd position, there are Nyquist dual-polarized 16QAM signals. Nyquist transmission is used to optimize bandwidth

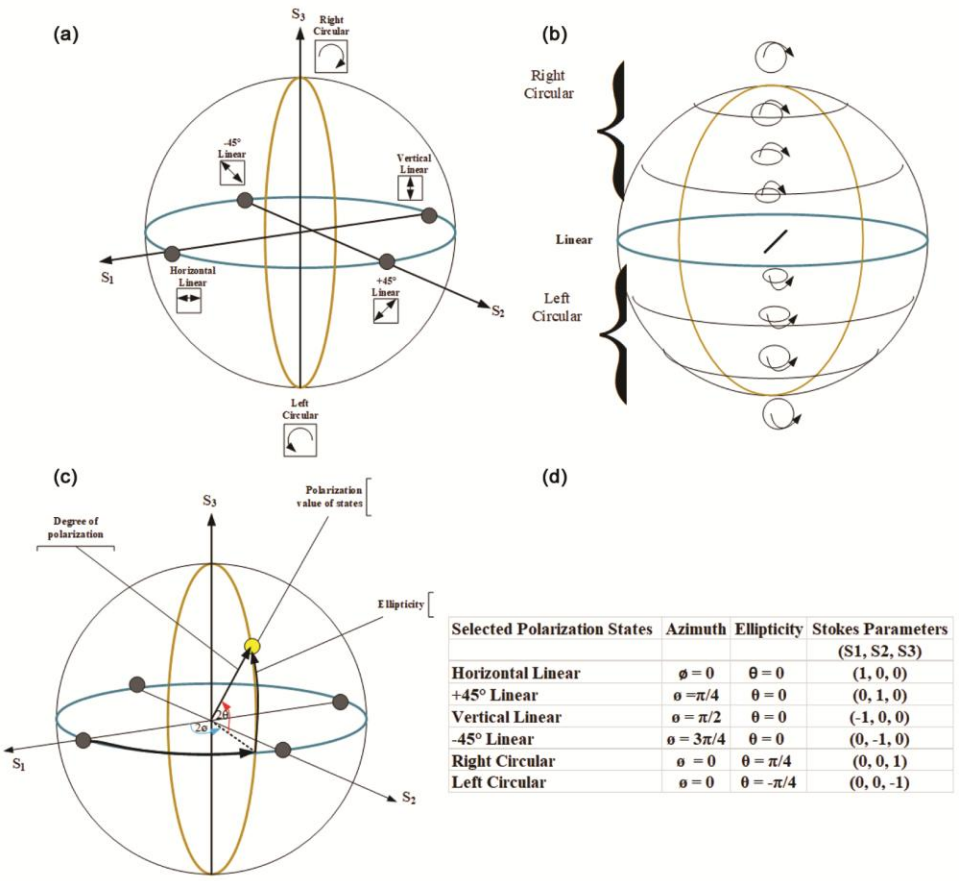

Selected Polarization States	Azimuth	Ellipticity	Stokes Parameters (S1, S2, S3)
Horizontal Linear	ø = 0	θ = 0	(1, 0, 0)
+45° Linear	ø =π/4	θ = 0	(0, 1, 0)
Vertical Linear	ø = π/2	θ = 0	(-1, 0, 0)
-45° Linear	ø = 3π/4	θ = 0	(0, -1, 0)
Right Circular	ø = 0	θ = π/4	(0, 0, 1)
Left Circular	ø = 0	θ = -π/4	(0, 0, -1)

Fig. 4 — (a) Poincare sphere showing various polarization states, (b) left and right circular polarization, (c) Polarization state values and stroke parameters in graphical, and (d) tabular form

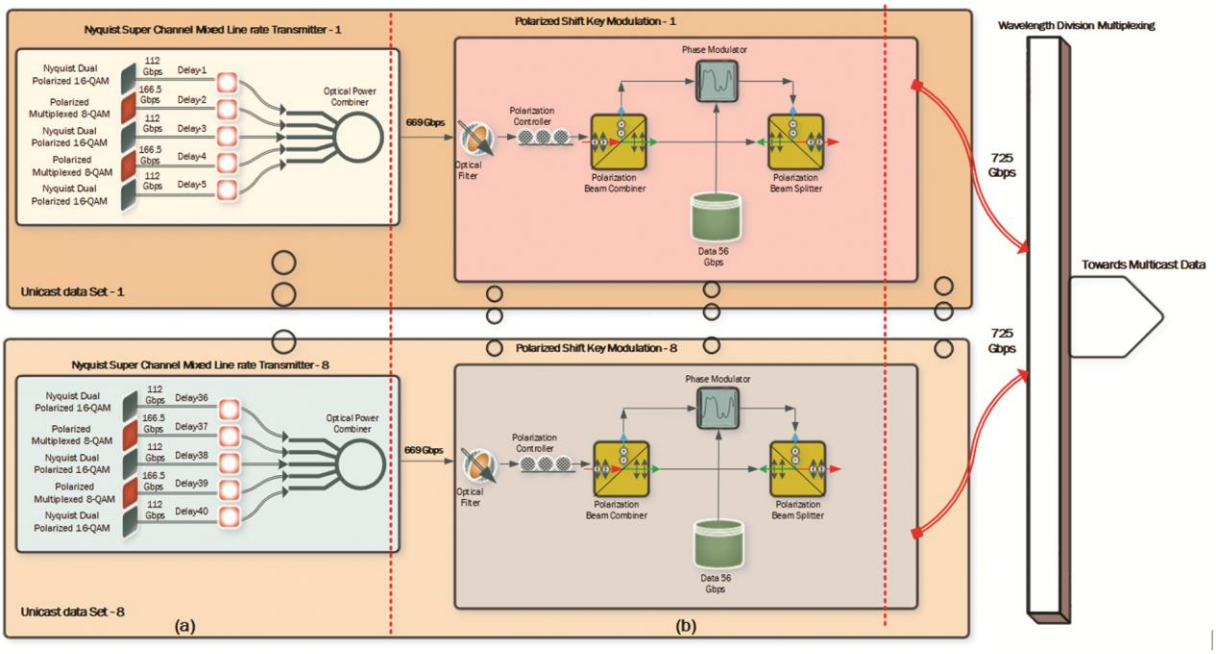

Fig. 5 — (a) Proposed Mixed line rate-based Nyquist WDM super-channel, and (b) with POLSK modulator

usage and also to obtain high spectral efficiency. The data rate used for transmission here is 112 G-bits/sec. random sequence generated NRZ type line coding is used. At an even position polarized multiplexed modulation 8QAM techniques were used. Each externally applied modulator consists of two Mach-Zehnder modulators in which driver signals are non-return to zero. The data rate used was 83.25 Gb/sec when dual applied to two external modulators giving a combined data rate of 166.5 Gb/sec. Now this combination of 5 channels combines to give a signal data rate of 669 Gb/sec, starting at a central frequency of 193.1 THz and other sub-carriers as. $193.1 \pm a.\Delta f_{Nyq}$ where a =1,2,3.. and Δf_{Nyq} is Nyquist channel spacing . To utilize the band efficiently and without having inter-symbol interference 15Ghz-20Ghz spacing is used. Now to provide proper shaping 4th-order Gaussian filter is used to give proper Nyquist pulse shaping. The subcarrier starts at 193.1 THz and ends at 193.160 THz. Nyquist channel spacing used is 15 GHz to have optimum use of bandwidth. Now after each data channel is properly modulated this combined data rate constitutes a single super-channel having a combined mixed modulated data rate into an optical combiner/ mixer by introducing an additional delay of 1-2 nano sec. Using an optical power mixer, it is passed through a polarized shift keying modulator as diagrammatically stated in Fig. 5(b). The combined mixed modulated WDM signal having data rate is fed into a Polarized shift keying module to create Unicast data. Now passing through an optical filter this combined data is fed into a polarization controller. This uniquely changes the state of polarization preferably at 45° and that is fed into Polsk. Now the detailing Polsk is being presented in Fig. 5(b). Here the polarization splitter splits the data one is fed directly into the polarization beam combiner other is fed into a phase modulation which is driven by an NRZ modulated 56 Gb/sec data. This splitting of data is none other than the splitting of components of electromagnetic waves which are mathematically represented in mathematical modelling as represented by Eqs (13) & (14). Now this whole modulation creates a single channel Unicast super channel WDM data having a speed of 669 Gb/sec + 56 G-bits/sec which is a 725 Gb/sec data rate. Now as mentioned earlier data coming out of a single Polsk constitutes a single Unicast data. Now to increase data capacity Each mixed line rate combination along with Polsk is further converted into 8 super-channels carrying data at a rate of 725 Gb/s from 193.1 THz to 193.8 THz. These 8 super-channels are further mixed multicast data. The modulator is used to superimpose the delayed unicast data with multicast data to avoid collision. Multicast. Data is prepared using 56 Gb/s data rate using differential quadrature phase shift keying as shown in Fig. 6. The combined WDM super channel unicast data fed into a Differential Quadrature Phase shift keying system in which NRZ line coding-based signal is used having a data rate of 56 G-bits/sec M-Ary provided biasing for Mach-Zehnder modulators. This hybrid modulated unicast and multicast data combination is now transferred to N loops circulated single mode and dispersion compensated fiber having an EDFA gain system.

Receiver side block diagram representation shown in Fig. 7. Firstly, unicast and multicast data are separated using an optical cross coupler -1 since mainly in these two forms data is primarily transmitted. Now since these data are polarization controlled there is provided polarization adjustment for both Unicast and multi-cast data.

Optical cross coupler–2 splits the Polsk Unicast data stream and 16QAM Nyquist polarized and 8QAM polarization multiplexed signals. For incoming Polsk light beam, is directed to the polarized beam adjuster which separates the light into two orthogonal components i.e., Vertical and horizontal components. Now for 16QAM Nyquist polarized and 8QAM polarization multiplexed signals recovery, before demodulation is done the five sub-channels are split by optical beam splitter and delays are nullified. The optical signal arrives at a receiver containing orthogonally polarized components each at 16QAM they employ a PBS to split into vertical and horizontal polarized components, and each polarized component is fed into a coherent receiver which uses a local oscillator to match the frequency of the incoming signal to enable to extract both magnitude and frequency information. The DSP processor corrects the dispersion-induced distortions, separates the horizontal vertical polarized components, and compensates for polarized mode dispersion, it mitigates any linear impairments and inter-symbol interference, extracts the phase and frequency information to properly demodulates the extracted signal, and maps the received constellation to respected data points.

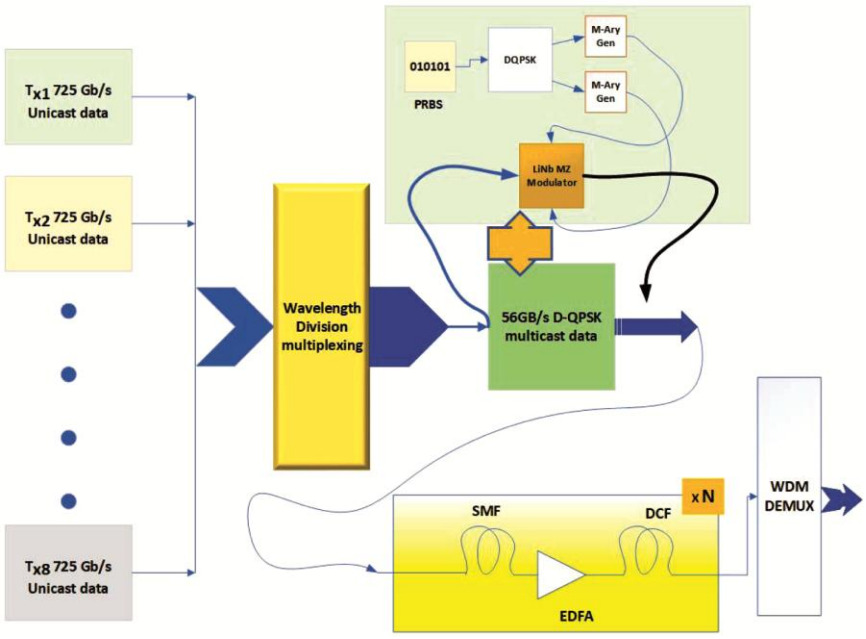

Fig. 6 — Multicast DQPSK based modulation

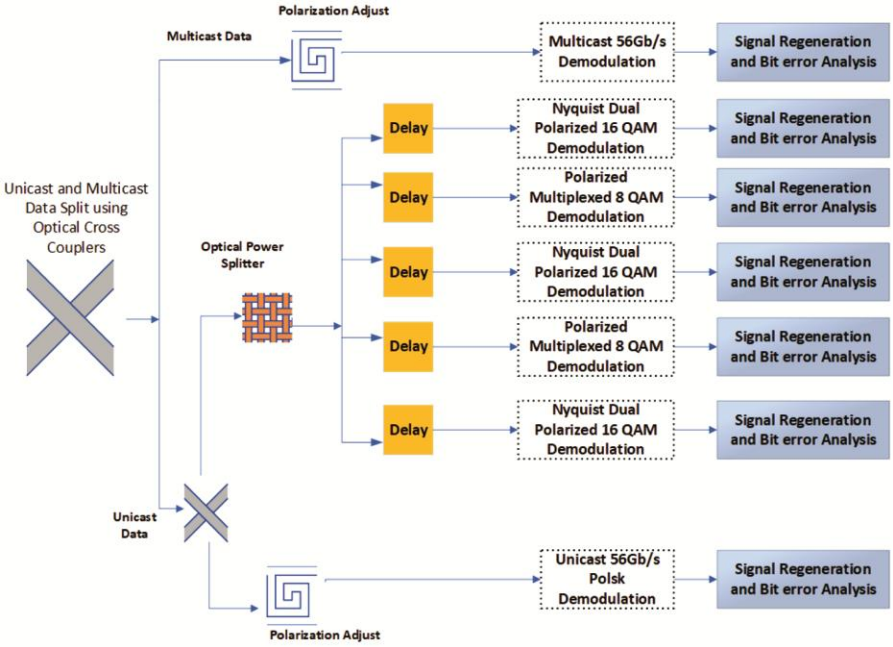

Fig. 7 — Receiver section

Results and Discussion

Received signal power and channel noise power at different frequencies is presented in Fig. 8(a). As each super-channel is centered around a frequency i.e., for reference Fig. 8 one particular super-channel is centered around 193.1 THz frequency. Likewise, all others channels till 193.8 THz, Fig. 8 shows the central frequency variation from all super-channels. Fig. 8(b) shows the optical signal-to-noise ratio versus the sub-carrier frequency graph. This parameter is used to measure the degree of signal over noise.

It represents a ratio of signal power over noise power within a stipulated bandwidth. Now when the optical signal is transmitted over a communication medium which in this case is optical fiber, there are certain due to various manufacturing processes so to compensate certain gains have to be inserted to compensate losses, for example path loss which is

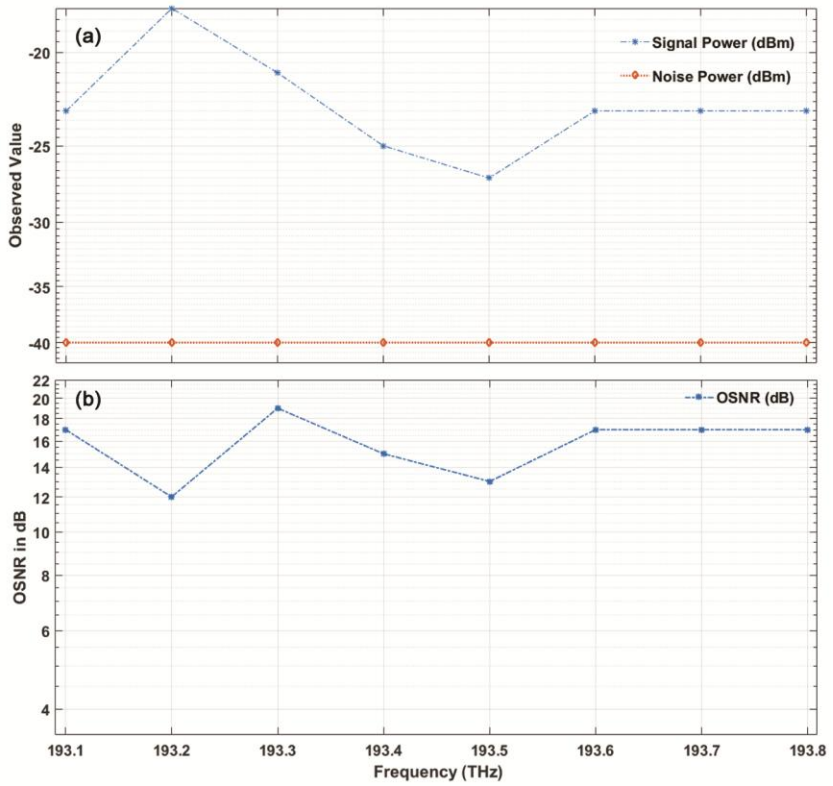

Fig. 8 — (a) Signal and Noise v/s subcarrier frequency, (b) OSNR v/s subcarrier frequency

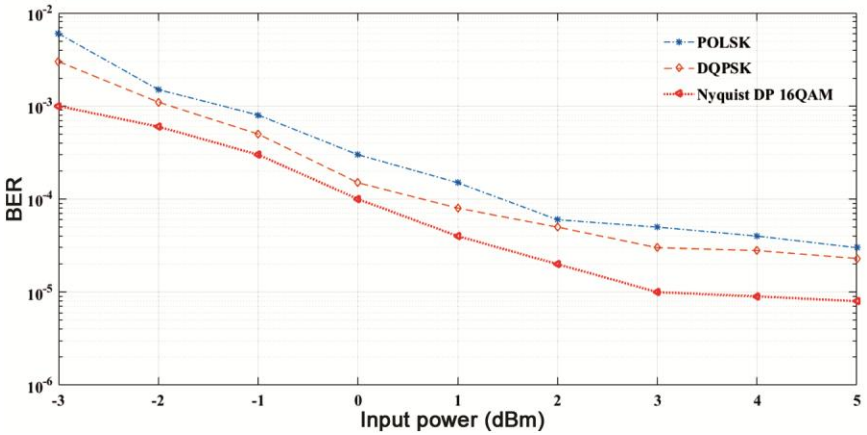

Fig. 9 — BER v/s Input Power

represented as dB/ Km so depending upon the fiber length that loss is compensated by providing that much gain. However, there is a constraint on using the number of optical amplifiers like EDFA because as amplifiers are increased, OSNR ratio is reduced. At the receiver the OSNR value is of utmost importance since low values of OSNR are an indication that the signal detected will be of low magnitude or even no signal will be detected. OSNR is numerical form is given as $OSNR_{signal} = \mathbf{10log}_{10}\left(\frac{P_{signal}}{P_{noise}}\right)$ where, P_{signal} is power received and P_{noise} is noise due to OFC properties.

In Fig. 9 there is a representation of bit error rate versus input power. In Fig. 9 all modulation formats are compared with input power variation. Now as per values obtained, it is observed that below 0 dB all three formats are above the standard bit error rate of 4×10^{-3} dB which means for power below 0 dB BER is

high and hence cannot be useful for practical transmission purposes. As the power increases beyond 0 dB all three modulation formats show improvement in BER and if all three are compared best performance is obtained in sequence as in decreasing order $BER_{DP-16QAM} > BER_{PM-8QAM} > BER_{DQPSK} > BER_{Polsk}$. The reason is that the modulation formats used, increase the data carrying capacity which in turn reduces the chances of bits getting lost or corrupted during transmission. Fig. 10 represents the performance comparison between the bit error rate and OSNR, for a fixed BER the performance of OSNR varies as best for DP-16QAM > PM-8QAM > DQPSK > Polsk. From Fig. 10 it is observed that for a fixed BER of 1×10^{-4} the best performance of OSNR is shown by the DP-16QAM Unicast system and lowest by Polsk. The comparison between the quality factor and various modulation formats with the distance covered as presented in Fig. 11 shows that the best Q for a particular distance is DP-16QAM and the lowest is obtained for Polsk the overall Q factor deteriorates as transmission distance increases.

The comparison between constellation diagrams and eye diagrams of various formats is also used. Fig. 5 represents DP-16QAM, PM-8QAM dense wavelength division multiplexing and this resultant super channel is transmitted further as a Unicast Data. The observed constellation diagrams are for distances 80 km, 300 km, and 550 km. As demonstrated from constellation diagrams signals for lesser distances have better signal resolve capability and as the distances increase the losses occurring within transmitting fiber due to losses become less resolved. In Fig. 12(a), the X-polarized and Y-polarized constellation diagram for a distance of 100 km is being demonstrated.

As observed from the comparative analysis of the constellations diagram for the DP-8QAM coherent receiver system in Fig. 12(b) as the received distance is increased, signal resolution is a little decreased and their distance from the central origin is reduced. When the received distance is further increased as shown in Fig. 12(c), the constellations are less resolved and more near towards the origin. As

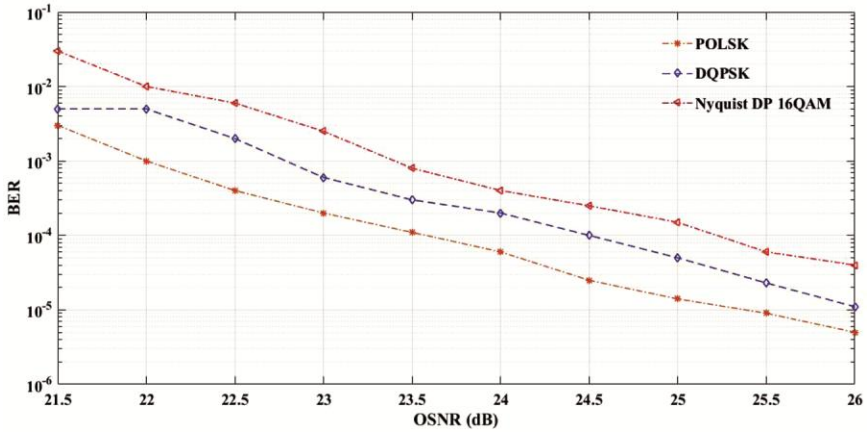

Fig. 10 — BER v/s OSNR

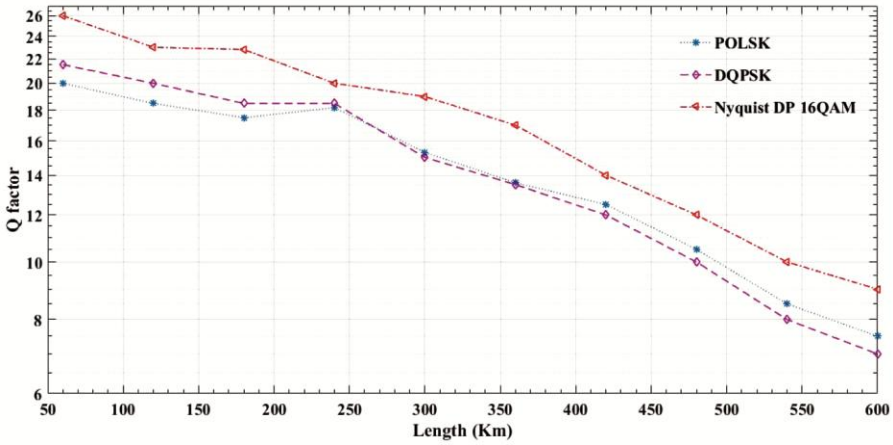

Fig. 11 — Q factor v/s length for each subcarrier

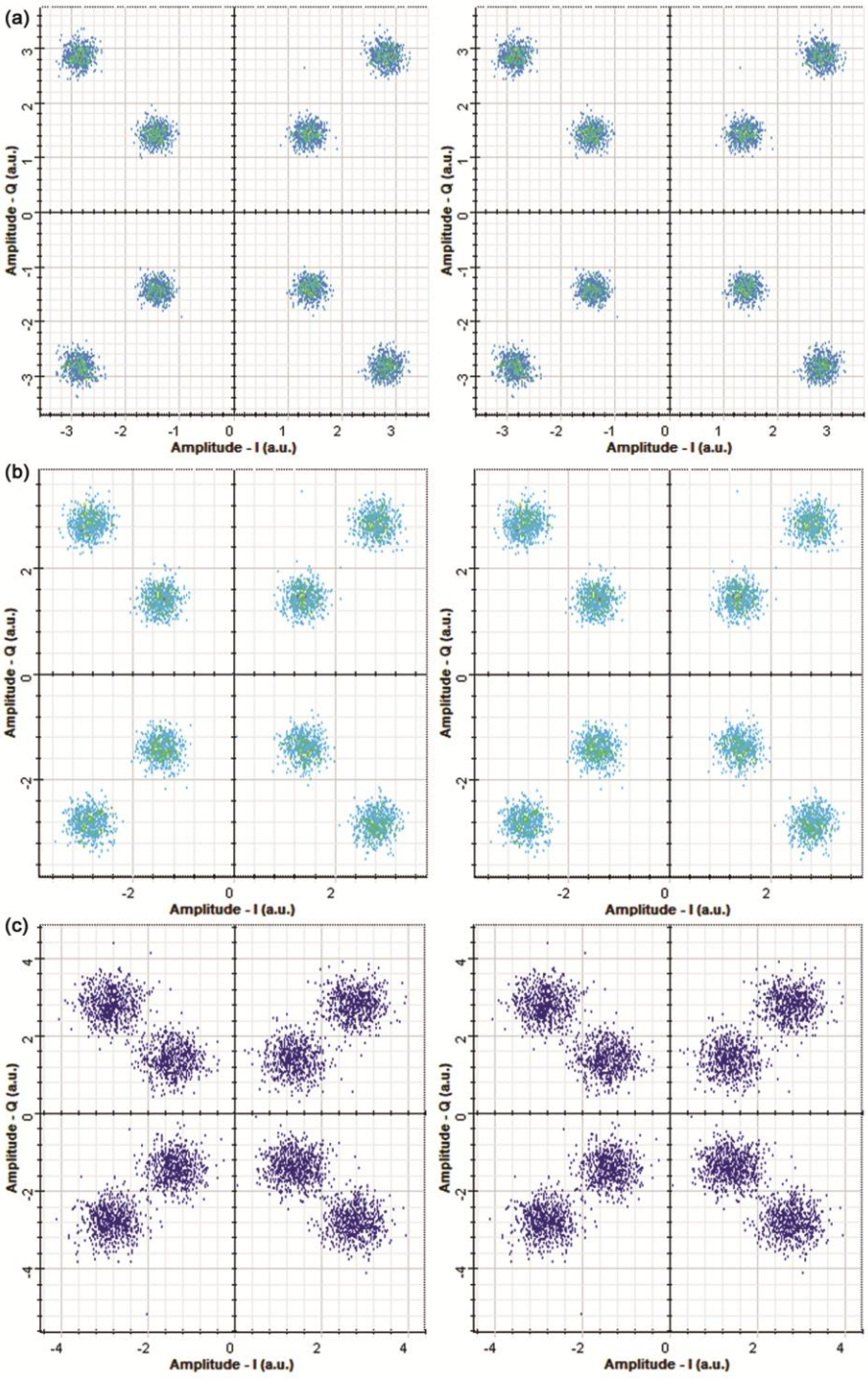

Fig. 12 — (a) DP-8QAM constellation at 100 Km, (b) DP-8QAM constellation at 300 Km and (c) DP-8QAM constellation at 550 Km

distances are increased the resolve clarity and distinguished signals get reduced. The given constellation diagrams show signal clarity as they are at the farthest point from the central point where these axes cross each other, which are primarily In-Phase and Quadrature phase magnitudes. To elaborate on various polarization states Poincare sphere and stroke parameters are utilized for each modulation format at various varying transmitting distances within optical fiber. The received polarization states for 8 QAM modulated signals at a distance of 100 Km are presented in Fig. 13(a) and (b). S_o represents the optical intensity of the polarized signal received. The theoretical analysis of stroke parameters has been

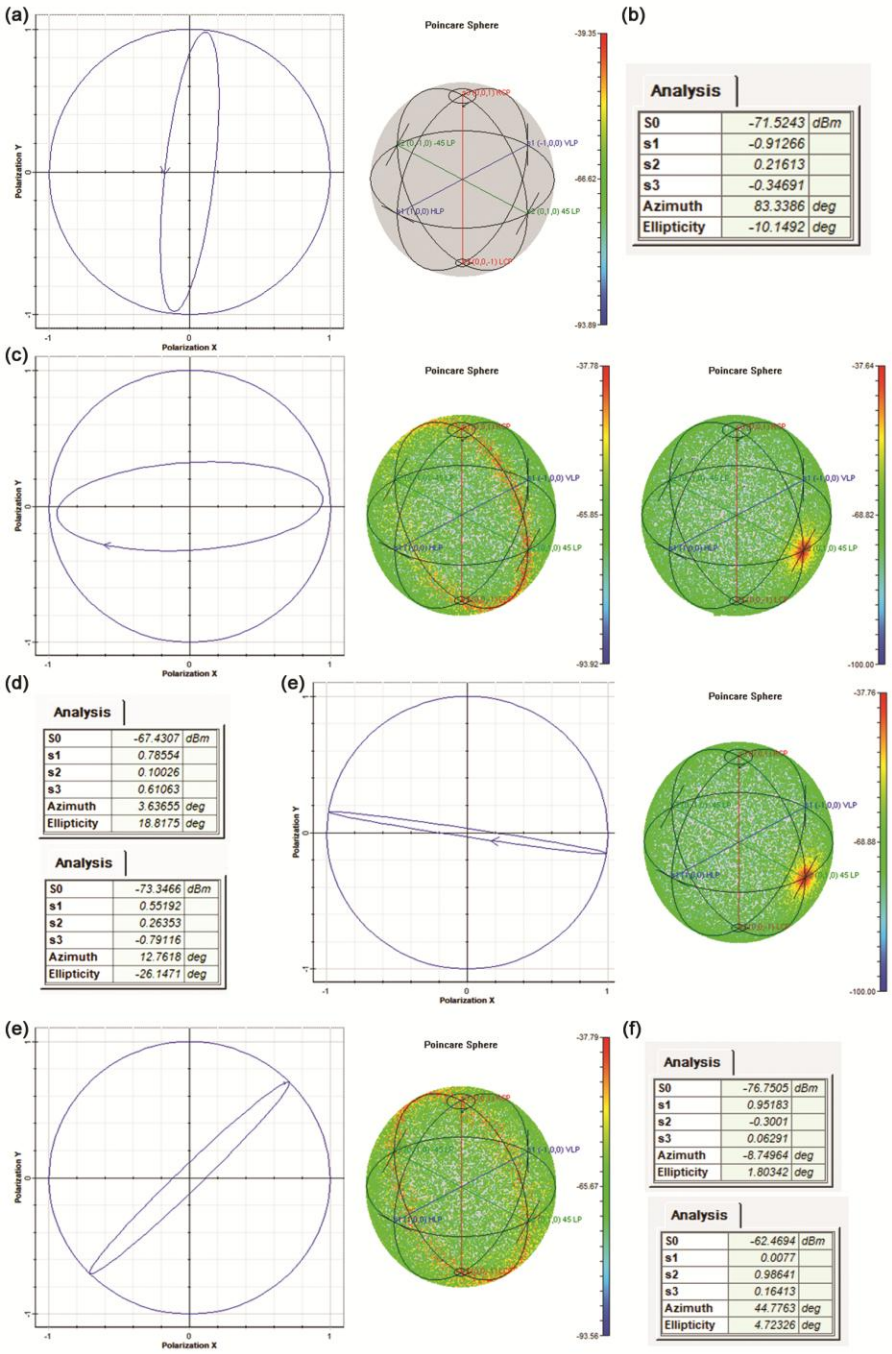

Fig. 13 — (a) DP-8QAM polarization states by Poincare sphere at 100 Km, (b) DP-8QAM polarization states at 100 Km strokes parameter values, (c) DP-8QAM polarization states by Poincare sphere at 300 Km transmitted and received states, (d) DP-8QAM stroke parameters values at 300 Km transmitted and received states, (e) DP-8QAM polarization states by Poincare sphere at 500 Km transmitted and received states, (f) DP-8QAM stroke parameters values at 500 Km transmitted and received states and.

taken in detail in Eqs (13–23). Polsk modulation hence concerning Eq. (16) and Fig. 4.

The azimuthal and elliptical states are also being shown for various travelled distances showing different orientations and magnitudes values. Now here S_{st1}, S_{st2}, and S_{st3} are being represented as s1, s2, and s3 in the simulation analysis observed. The s1 value is negative which means that it is linearly polarized in the x direction, s2 indicates that there will be +45° inclination in the x direction. s3 negative value indicates that it is left-circularly polarized. Furthermore, the values of Azimuth and Ellipticity

indicate the inclination as more validated from the arrow on the elliptical diagram and Poincare sphere. Further same is shown for distances of 300 Km through the Poincare sphere in Fig. 13(c) and (d) and 500 Km through Fig. 13(e) and (f).

Now another important parameter of evaluation received signal is in the form of eye pattern which has relative value of quality factor values as well as bit error rate evaluation. A relative comparison of the mixed line rate eye diagram pattern for D-QPSK, PM-8QAM, and DP-16QAM for a distance of approx. 500 Km and 600 Km is demonstrated in Fig. 14. The eye diagram patterns shown in Fig. 14(a) and Fig. 14(b) here are of mixed line rate flexible transmission systems. Now as the symbol rate in the D-QPSK system is two, the symbol rate for PM-8QAM is 3 for the DP-16QAM system is four as it's observed that the increase in M-Ary values of given modulation formats then for a given commonly transmitted distance since data carrying capacity is increased by higher order modulation formats hence the eye closure response is accordingly, which concludes that as for a fixed transmission distance data carrying capacity is increased eye pattern opening get reduced accordingly, as shown in Fig. 14(a) and Fig. 14(b). The parameters employed in this research are rated in Table 1.

Comparison of the current work with earlier similar or related work is given in Table 2 with reference to various parameters used for the evaluation of the performance of earlier systems. Bosco *et al.*[7] reported a transmission capacity of 1.1 Tbps and spectral efficiency of 4.6 bits/s/Hz compared to the proposed system whose data carrying capacity is about 5 times higher with spectral efficiency increase of 1.13 times. When compared with Silva *et al.*[14] it is observed that there is slight reduction in spectral efficiency values and almost 12 times increased data carrying capacity. Similarly, in comparison to Pincemin *et al.*[18], there is reduction of half value in spectral efficiency but approx. 10 times increase in data carrying capacity. Compared to Singh *et al.*[20], approx. 20% improvement in spectral efficiency and a significant improvement of 12 times in transverse distance is observed, while in Singh *et al.*[23], approx. 40% improvement in spectral efficiency is observed.

Table 1 — Various fiber parameter values used for two variations of Fiber used in this system

Optical Fiber parameters SSMF PSCF	Optical Fiber parameters SSMF	Optical Fiber Parameters DCF
Attenuation per km (α) in dB/km	0.22	0.168
Total fiber length in km	50	10
Total fiber length loss in dB/km	19.8	15.12
Chromatic dispersion at 1550 nm in ps/ nm/km	16.7	20.5
Dispersion slope in ps/nm2/km	0.07	0.059
Effective area in μm^2	78	110
Nonlinear coefficient in $W^{-1} \cdot km^{-1}$	1.3	1.0318

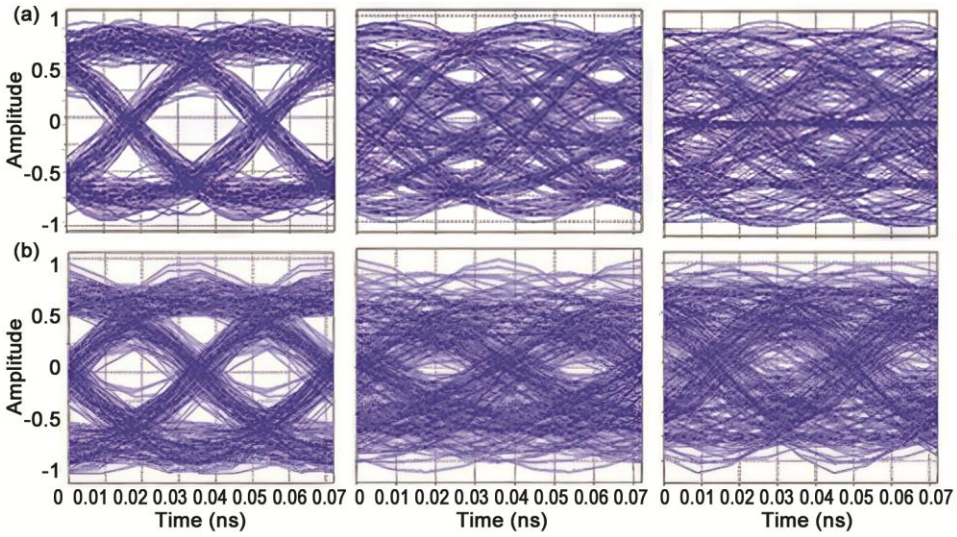

Fig. 14 — Eye diagram pattern for MLR WDM super-channel for D-QPSK, PM-8QAM, and DP-16QAM at distances of (a) 500 Km and (b) 600 Km respectively

Table 2 — Proposed work with similar work based on Nyquist super-channel and Mixed Line rate

Parameters ↓	Bosco *et al.*[7]	Silva *et al.*[14]	Xie *et al.*[17]	Weng *et al.*[25]	Pincemin *et al.*[18]	Singh *et al.*[20]	Singh *et al.*[23]	Proposed work
Modulation formats utilized	PM-8QAM, PM-16QAM	PDM-16QAM	PDM-16QAM and PDM-QPSK	PM-64QAM	PM-BPSK, PM-QPSK, PM-8QAM, PM-16QAM	DP-16QAM, Polsk, DPSK Multicast Overlay system	PM-8QAM, PM-16QAM	D-QPSK, PM-8QAM, DP-16QAM, Unicast Polsk, and Multicast Overlay system
Data transmitted rate (Gb/s)	7×166.5, and 5×222	448	260 and 130	3×336	1×55.5, 1×111, 1×166.5, 1×222	35×105	2×166.5, 3×222	2×166.5, 3×112,
Utilization of Super-channel	Nyquist WDM	—	Nyquist Pulse Shaping	—	MLR-based Nyquist WDM	Nyquist Super-channel	MLR mixed Nyquist WDM	MLR combined Nyquist Dense Multiplexing,
Channel spacing used (GHz)	33.33	75	50	27	33.33	25	33.33	15
Spectral efficiency (bits/s/Hz)	4.6	6.2	5.6	5.2 and 2.6	12.4	4.2	3.75	5.2
System data carrying capacity (Tb/s)	1.1	0.448	0.260 and 0.130	0.996	0.55	3.5	1	5.856
Type of Optical Fiber Used	SSMF	SSMF	SSMF and DCF	SSMF	PSCF	SSMF and DCF	SSMF and PSCF	SSMF and DCF
Reach (km)	1150, 520	678	960 and 4160	80	2800 2100 1650 1040	50	3100, 1600, 3600, 2200	600
Spectral efficiency distance product (bits/s/Hz-Km)	5290, and 3224	3796	4992 and 10816	992	11648, 8736, 6864, 4326	187.5	16120, 8320, 18720, 11440	5570

Conclusions

Analysis of the results indicates significant decreases in bit error rate observed after 0 dB input power, with acceptable BER levels reaching up to 5 dB, further upon examining the bit error rate and optical signal-to-noise ratio (OSNR), it is evident that unicast data transmission outperforms multicast data transmission. Specifically, at an OSNR value of 26 dB and a bit error rate of 5×10^{-5}, the performance of unicast 16 QAM significantly surpasses that of multicast modulation. Analyzing the Q factor for the distance travelled, one can see that even at 600 km, the Q factor remains good, and unicast data transfer performs significantly better than multicast data transmission. Along with high data capacity transmission across a distance of 600 Km, high data capacity, lower BER, high-quality factor value, and high spectral efficiency for overlay multicast and unicast data sending is acquired. Further analysis of the proposed scheme might include more complex higher modulation formats (e.g., 64-QAM) incorporating greater amounts of bits per symbol although having reduced Euclidean spacing across constellation locations requiring higher OSNR for accurate detection of higher-order modulated signals. Heterogeneous modulation schemes generate varying symbol speeds and spectral imprints. Disparities in spectral widths may lead to spectral misalignment, necessitating advanced adaptive filters and Nyquist pulse structuring. By interacting with SDN-based optical control, the network may dynamically allot bandwidth and change modulation formats in response to traffic demands.

References

1 Yadav U & Thangaraj J, Review and analysis of elastic optical network and sliceable bandwidth variable transponder architecture, *Opt Eng*, **57(11)** (2018) 110802, https://doi.org/10.1117/1.OE.57.11.110802.

2 Danish R, Talha R, Antonio N, Maxim K, Gottfried L & Bernhard S, Flex-grid optical networks: spectrum allocation and nonlinear dynamics of super-channels, *Opt Express*, **21** (2013) 32184–32191, https://doi.org/10.1364/OE. 21.032184.

3 Amar D, Brochier N, Le Rouzic E, Auge J L, Lepers C, Cousin B & Kanj M, Link design and legacy amplifier

limitation in flex-grid optical networks, *IEEE Photonics J*, **8** (2016) 1–10, https://doi:10.1109/jphot.2016.2527023.

4 Chatterjee B C & Sharma O E, Routing and spectrum allocation in elastic optical networks: a tutorial, *IEEE Commun Surv Tutor*, **17** (2015) 1776–1800, https://doi.org/10.1109/COMST.2015.2431731.

5 Christodoulopoulos K, Tomko I & Varvarigos Z, Elastic bandwidth allocation in flexible OFDM-based optical networks, *J Light Technol*, **29** (2011) 1354–1366, https://doi.org/10.1109/JLT.2011.2125777.

6 Rival O & Morea A, Elastic optical networks with 25–100 G format-versatile WDM transmission systems, *OECC 2010 Technical Digest*, (2010) 100–101, https://doi.org/10.1109/COMST.2015.2431731.

7 Bosco G, Curri V, Carena A, Poggiolini P & Forghieri F, On the performance of Nyquist-WDM terabit super-channels based on PM-BPSK, PM-QPSK, PM-8QAM or PM-16QAM subcarriers, *J Light Technol*, **29** (2011) 53–61, https://doi.org/10.1109/JLT.2010.2091254.

8 Ashraf M W, Idrus S M, Butt R A & Iqbal F, Post-disaster least loaded light path routing in elastic optical networks, *Int J Commun Syst*, **32(8)** (2019) 3920, https://doi.org/10.1002/dac.3920.

9 Meng X, Songnian Fu, Ming T, Haoyuan T, Perry S & Deming L, Nyquist WDM super-channel using offset-16QAM and receiver-side digital spectral shaping, *Opt Express*, **22** (2014) 17448–17457, https://doi.org/10.1364/OE.22.017448.

10 Shao Y & Chi N, High spectral-efficiency 100Gbit/s transmission using DRZ, DQPSK, and PoLSK three-dimension orthogonal modulation, *Opt Commun*, **285(6)** (2012) 1049–1052, https://doi.org/10.1016/j.optcom.2011.11.076.

11 Devi S, Sharma D & Prajapati Y K, 5×222 Gb/s PM-16QAM Nyquist-WDM super channel, *SUSCOM-2019*, (2019) 357–362, https://doi.org/10.2139/ssrn.3351800.

12 Zhang J, Dong Z, Chien H C, Jia Z, Xia Y & Chen Y, Transmission of 20×440-Gb/s super-Nyquist-filtered signals over 3600 km based on single-carrier 110-GBaud PDM QPSK with 100-GHz grid, *OFC 2014*, (2014) 1–3, https://doi.org/10.1364/OFC.2014.TH5B.3.

13 Roberts K, Foo S, Moyer M, Hubbard M, Sinclair A, Gaudette J & Laperle C, High-capacity transport – 100G and beyond, *J Light Technol*, **33** (2015) 563–578, https://doi.org/10.1109/JLT.2014.2358203.

14 Jia Z, Chien H, Zhang J, Cai Y & Yu J, Performance comparison of dual-carrier 400G With 8/16/32-QAM modulation formats, *IEEE Photonics Technol Lett*, **27(13)** (2015) 1414–1417, https://doi.org/10.1109/LPT. 2015. 2423613.

15 Sharma D, Prajapati Y & Tripathi R, Success journey of coherent PM-QPSK technique with its variants: a survey, *IETE Tech Rev*, **37(1)** (2018) 36–55, https://doi.org/10.1080/02564602.2018.1557569.

16 Rahman T, Rafique D, Spinnler B, Pincemin E, Le Bouette C, Jauffrit J, Calabrò S, de Man E, Bordais S, Feiste U, Slovak J, Napoli A, Khanna G, Hanik N, Andre C, Okonkwo C M, Kuschnerov M, Koonen A M, Dourthe C, Raguenes B, Sommerkorn-Krombholz B, Bohn M & de Waardt H, Record field demonstration of C-band multi-terabit 16–QAM, 32–QAM and 64–QAM over 762 km of SSMF, *OECC 2015*, (2015) 1–3, https://doi.org/10.1109/OECC.2015.7340292.

17 Xie C, Raybon G & Winzer P J, Transmission of Mixed 224-Gb/s and 112-Gb/s PDM-QPSK at 50-GHz channel spacing over 1200-km dispersion-managed LEAF® spans and three ROADMs, *J Light Technol*, **30(4)** (2012) 547–552, https://doi.org/10.1109/jlt.2011.2176313.

18 Pincemin E, Loussouarn Y, Gautier S, Chen Y, Yuan W, Hong Y, Wei X & Dejiang Z, Single-carrier and multi-carrier 400 Gbps transmission with multi-rate, multi-format real-time transceiver prototypes, *J Light Technol*, **37** (2019) 524–537, https://doi.org/10.1109/JLT.2018.2874106.

19 Rahman T, Rafique D, Napoli A, de Man E, Spinnler B, Bohn M & de Waardt H, Ultralong haul 1.28-Tb/s PM-16QAM WDM transmission employing hybrid amplification, *J Light Technol*, **33(9)** (2015) 1794–1804, https://doi:10.1109/jlt.2015.2401836.

20 Singh S, Bandwidth efficient hybrid modulation technique in the scenario of 3.5 Tb/S dense wavelength multiplexed system, *OAM-RC*, **11(1-2)** (2017) 51–53

21 Xia T J, Wellbrock G A, Tanaka A, Huang M, Huang Y, Zhang S, Zhang Y, Aono Y, Murakami S & Tajima T, High-capacity field trials of 40.5 Tb/s for LH distance of 1,822 km and 54.2 Tb/s for regional distance of 634 km, *(OFC/NFOEC)*, (2013) 1–3, https://doi.org/10.1364/NFOEC.2013.PDP5A.4.

22 Pincemin E, Loussouarn Y, Gautier S, Chen Y, Yuan W, Hong Y & Dejiang Z, Single-carrier and multi-carrier 400 Gbps transmission with multi-Rate multi-format real-Time transceiver prototypes, *J Light Technol*, **37** (2019) 524–537, https://doi.org/10.1109/JLT.2018.2874106.

23 Singh S, Singh S, Ngo Q M & Mohammadi A M, 340-Gb/s PolSK-DP-DQPSK optical orthogonal modulation format with coherent direct detection for high capacity WDM optical network, *Opt Fiber Technol*, **52** (2019) 101936, https://doi.org/10.1016/j.yofte.2019.101936.

24 Loussouarn Y, Pincemin E, Gautier S, Chen Y, Yuan W, Hong Y, Wei X & Jiang Z, Single-Carrier 61 Gbaud DP-16QAM transmission using bandwidth-limited DAC/ADC and narrow filtering equalization, *OFC 2017*, (2017) 1–3, https://doi.org/10.1364/oe.23.018988.

25 Shao Y & Chi N, High spectral-efficiency 100Gb/s transmission using DRZ, DQPSK and PoLSK three-dimension orthogonal modulation, *Opt Commun*, **285(6)** (2012) 1049–1052 https://doi.org/10.1016/j.optcom.2011.11.076.